Monsoon variability and deep oceanic circulation in the western equatorial Pacific over the last climatic cycle: Insights from sedimentary magnetic properties and sortable silt

Catherine Kissel,[1] Carlo Laj,[1] Markus Kienast,[2] Timothé Bolliet,[3] Ann Holbourn,[3] Paul Hill,[2] Wolfgang Kuhnt,[3] and Pascale Braconnot[1]

Received 20 April 2010; accepted 8 June 2010; published 29 September 2010.

[1] Magnetic and grain size properties of a sediment core located in the western equatorial Pacific, off the southeastern tip of the Philippine island of Mindanao, are presented in an effort to reconstruct past changes in the East Asian Monsoon and deep ocean circulation during the last 160 kyrs. The sedimentary concentration of magnetic particles, interpreted to reflect past changes in runoff from Mindanao, varies almost in antiphase with Northern Hemisphere insolation. This suggests that precipitation was lower in the western equatorial Pacific region during boreal insolation maxima and thus corroborates model results showing opposing trends in precipitation between land and the marine realm there. Variations in the grain size distribution of the inorganic sediment fraction, as recorded by both the sortable silt mean size and the magnetic grain size, provide a monitor of changes in sediment reworking by bottom currents. The close correlation of this proxy of bottom current strength and the benthic $\delta^{18}O$ record from the same site implies a tight coupling between deep water flow, most likely Antarctic Intermediate Water (AAIW), and global climate.

Citation: Kissel, C., C. Laj, M. Kienast, T. Bolliet, A. Holbourn, P. Hill, W. Kuhnt, and P. Braconnot (2010), Monsoon variability and deep oceanic circulation in the western equatorial Pacific over the last climatic cycle: Insights from sedimentary magnetic properties and sortable silt, *Paleoceanography*, *25*, PA3215, doi:10.1029/2010PA001980.

1. Introduction

[2] The western equatorial Pacific is a key area for understanding past climate variability and interactions between high and low latitudes. This region is affected by seasonal climate variations dominated by fluctuations in precipitation due to the migration of the Intertropical Convergence Zone (ITCZ) resulting in the seasonal march of the monsoon and interannual changes in precipitation patterns associated with the El Niño/Southern Oscillation (ENSO) phenomenon. Moisture and latent heat from these areas are distributed throughout the globe via large−scale atmospheric circulation. Their role in the global oceanic circulation and in particular the thermohaline circulation is fundamental, due to the salinity gradient with respect to high latitudes. Therefore, the western equatorial Pacific is a critical area for assessing the role of the oceanic circulation in the transfer between high and low latitudes climatic changes and in the heat and moisture transport and distribution.

[3] We report here on a detailed study of the magnetic properties and grain size in a core (IMAGES core MD06-3067) taken at the southeastern tip of Mindanao [*Laj et al.*, 2006]. This area appears particularly relevant because it is affected by the East Asian Monsoon, the position of the ITCZ, and it is also a critical area for understanding past changes in the dynamics and in the pathways of the main oceanic water masses (Figure 1). While the present-day patterns of surface and subsurface currents are relatively well documented, very little is known for deeper currents. It may be hypothesized, however, that water masses formed at high southern latitudes reach this region and thus directly transmit some high-latitude fluctuations to low latitudes. This was recently suggested by *Saikku et al.* [2009] in a submillennial-scale study of marine isotopic stage 3 in IMAGES core MD98-2181, located within the Davao Bay. Our core, located in the open West Pacific, is well suited for reaching our objectives which are (1) monitoring changes in the monsoon activity via precipitation on land and the resultant sedimentary discharge and (2) investigating past variations in bottom current flow and their relationship with high-latitude circulation patterns.

2. Oceanographic and Climatic Setting

[4] From an oceanographic point of view, the southern Mindanao area is called the "water mass cross roads" [*Fine et al.*, 1994], because several water masses from the northern and southern hemispheres meet there (Figure 1).

[1]Laboratoire des Sciences du Climat et de l'Environnement/IPSL, CEA-CNRS-UVSQ, Gif-sur-Yvette, France.
[2]Department of Oceanography, Dalhousie University, Halifax, Nova Scotia, Canada.
[3]Institut für Geowissenschaften, Christian-Albrechts-Universität, Kiel, Germany.

0883-8305/10/2010PA001980

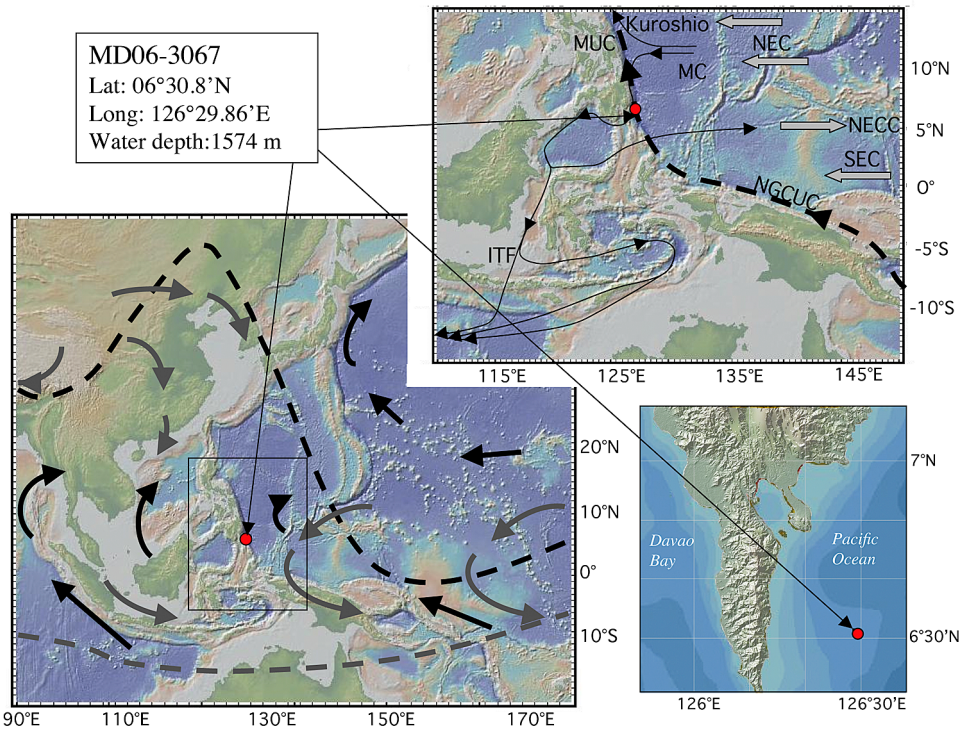

Figure 1. Maps showing the location of core MD06-3067. (left) Summer (dashed black line) and winter (dashed gray line) positions of the ITCZ and associated directions of trade winds. (top right) Main oceanic water masses (MC, Mindanao Current; MUC, Mindanao Undercurrent; NGCUC, New Guinea Coastal Undercurrent; ITF, Indonesian Throughflow; NEC, North Equatorial Current; NECC, North Equatorial Counter Current; SEC, South Equatorial Current). (bottom right) More precise location of the core with respect to the southern tip of Mindanao and the Davao Bay. The maps are constructed using GeoMapApp software.

The southward flowing Mindanao surface current (MC) originates from the North Equatorial Current at about 15°N. It has a near-surface speed at present of about 1m/s on the average and experiences a vertical shear in the upper 300 m with a net transport increasing from north to south to attain a maximum of about 33Sv at the latitude of south Mindanao [*Toole et al.*, 1990; *Lukas et al.*, 1991]. South of Mindanao, part of this current flows into the Celebes Sea and passes through a complex array of passages within the Indonesian archipelago to arrive in the Indian Ocean (the Indonesian Throughflow, ITF). The other part turns eastward and contributes to the North Equatorial Counter Current. It probably also gives rise to the Mindanao Eddy.

[5] At intermediate depth below the MC (i.e., depths > 400–600 m), the Mindanao Undercurrent (MUC) is connected to the strong northwestward flowing deep layer of the New Guinea Coastal Under Current (NGCUC) (Figure 1). The latter, originating from the Northeastern coast of Australia [*Lindstrom et al.*, 1987], merges with the southern-sourced Antarctic Intermediate Water (AAIW) and the deep part of the South Pacific Tropical Water and flows along the New Guinea northern coast from the Solomon Sea [*Tsuchiya*, 1991]. At present, the retroflection flow of the MC from the Celebes Sea prevents the upper part of the NGCUC to flow northward [*Kashino et al.*, 1996] while its deep part is free to pass. *Tsuchiya* [1991] demonstrated the role played by the NGCUC as the pathway of the AAIW into North Pacific. The CTD profile we obtained at the location of core MD06-3067 is very similar to the one reported by *Lukas et al.* [1991, Figure 10] with very uniform temperature and salinity properties between 600 and 1500 m, with the salinity reaching about 34.6 psu at 1500 m. In the nearby WOCE E-W (P04) and N-S (P08) profiles all the chemical properties (temperature, salinity, silica, oxygen) are also very uniform at these depths [*Talley*, 2007]. *Broecker et al.* [1986] showed nearly unchanged oxygen concentrations between 1360 and 1790 m water depth in a water column profile to the south of our coring site (5°S/128°E). Taken together, these scarce water column profiles and interpretations available to date suggest a homogenous water mass between 600 and 1800 m off Mindanao, most likely reflective of northward flowing AAIW.

[6] The climate of the southern Mindanao region is strongly influenced by the East Asian monsoon induced by seasonal changes in the pressure gradient and resulting from the different potential heating between the ocean and the Asian continent (Figure 1). Presently, heating of the Asian continent during boreal summer gives rise to a strong inflow of air from ocean to land. These strong winds result from the low-pressure cell over the Asian continent, and cause

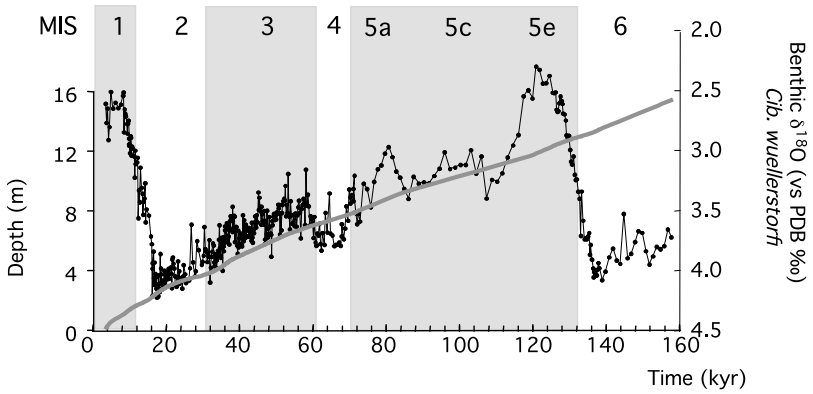

Figure 2. Benthic oxygen isotope record and age-depth relationship (gray line) in core MD06-3067. MIS stands for marine isotopic stages.

rainfalls over southern Asia (i.e., the summer monsoon). The East Asian summer monsoon is associated with a very significant northward migration of the rain belt up to 45°N. In boreal winter, the situation is reversed with more arid conditions on the continent and displacement of the ITCZ to about 10–15°S. The strength of the monsoon has undergone large changes in the past and it is widely recognized that they were largely forced by insolation [*Wang et al.*, 2005]. However, the debate is still active, depending on the region studied and the oceanic or continental proxies used, whether only precession or both precession and obliquity control the monsoon regime. As noted by *Wang* [2009, p. 1119], "the specific sea-land settings of the regions may bring about different monsoon responses to the same orbital forcing." This results from the fact that the monsoon is a large-scale phenomenon and therefore, shifts in the monsoon system lead to increase in precipitation rate in some areas and to decrease in others.

3. Core Site and Sample Material

[7] Core MD06-3067 was recovered during the IMAGES XIV-MD155-Marco Polo 2 cruise on board the R. V. *Marion Dufresne* of the French Polar Institute (IPEV) [*Laj et al.*, 2006]. The core site is located at 06°30.86′N and 126°29.86′E, 1574 m water depth, in the open western equatorial Pacific at the southeastern tip of the Philippines, off the island of Mindanao (Figure 1). The 15.53 m long CALYPSO core is composed of medium olive gray silty clay with some pumice pebbles (up to 1 cm). An ash layer is present at 198–200 cm.b.s.f.

[8] Directly on board, a fiducial line was drawn along the plastic tube containing the sediment before cutting the core into 1.5 m segments. So, although the core was not azimuthally oriented, the relative orientation of the different segments was preserved to within about 5°. These segments were then split longitudinally into two halves, taking care to cut along the fiducial line.

[9] The archive half of the core was scanned for major element intensities using the Avaatech XRF core scanner [*Richter et al.*, 2006] at Bremen University. The working half was entirely sliced into 1 cm thick samples for the analysis of foraminifera at the University of Kiel. Two types of samples were taken for magnetic analyses. First, the archive half of the core was sampled continuously using 2 × 2 × 150 cm u channels [see, e.g., *Weeks et al.*, 1993]. In addition, standard 2 × 2 × 2 cm plastic cubic boxes were used to obtain samples for the study of the anisotropy of the susceptibility. Finally, small amounts (ca. 0.2 g) of sediments were also taken every 10 cm for the magnetic hysteresis measurements and first-order reversal curves (FORC) analyses. Following the magnetic analyses at LSCE, the u channels were shipped to Dalhousie University, where subsamples taken every 10 cm were used for determination of the disaggregated inorganic grain size composition.

4. Results

[10] The age model of core MD06-3067, presented in detail in T. Bolliet et al. (submitted to *Paleoceanography*, 2010), is based on seven ^{14}C AMS dates for the upper 420 cm (ca. 34 kyr) of the core and on correlation of the benthic oxygen isotope record obtained from the epifaunal benthic foraminifera *P. wuellerstorfi* (see Figure 2) with the EDML reference δ^{18}O record [*Ruth et al.*, 2007]. An age adjustment of 1000 years [*Stott et al.*, 2007] is made for benthic age tiepoints to compensate for the travel time of the benthic oxygen isotope signal from the Southern Ocean to the Mindanao site. A detailed description of the methods used to characterize the magnetic properties and the disaggregated inorganic grain size composition is given in Appendix A. We focus here on the meaning of the used parameters in terms of nature, grain size and concentration of the magnetic particles and sortable silt mean size. We shall then discuss the variations observed in these parameters in terms of climatic and oceanic circulation changes in this region.

4.1. Magnetic Assemblage and Major Elements

[11] The nature of the magnetic particles has been investigated using different parameters and properties (see Appendix A). First, the coercivity parameters, S-ratio$_{-0.3T}$, Hmd_{ARM} and Hmd_{IRM} are very uniform all along the core with values around 0.98, 23 mT and 12 mT, respectively,

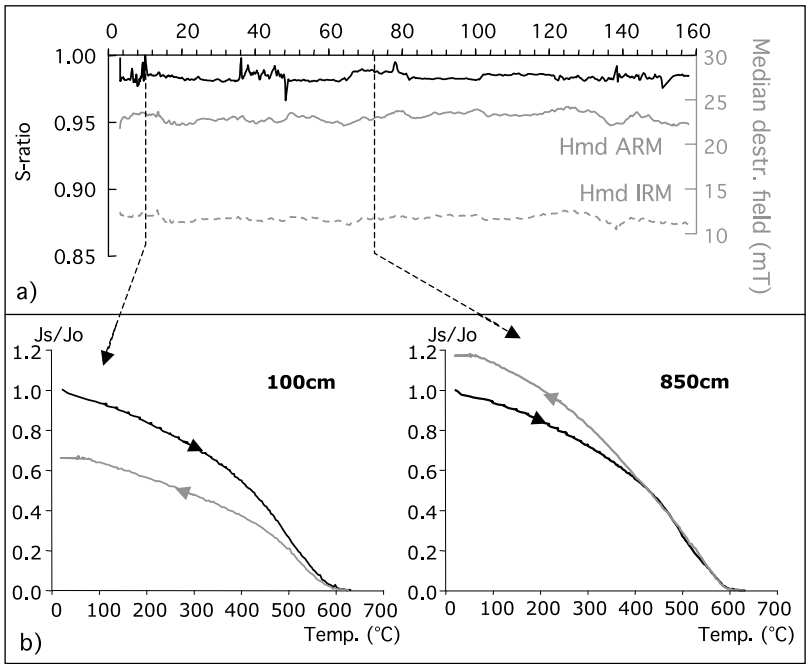

Figure 3. Magnetic parameters defining the magnetic mineralogy in core MD06-3067. (a) S-ratio$_{-0.3T}$ (black line) and median destructive fields of ARM and IRM (Hmd_{IRM} in dashed gray line and Hmd_{ARM} in continuous gray line); (b) two representative thermomagnetic curves obtained from different horizons with the heating curve in black and the cooling curve in gray. All indicate that the main carrier is low Ti content magnetite.

indicating that only low-coercivity magnetic minerals are present in the core (Figure 3a). Thermomagnetic experiments on samples at different depths all reveal a progressive decay of the saturation magnetization upon heating until a complete loss of magnetization around 580–600°C (Figure 3b). The subsequent cooling curve has the same shape, sometimes slightly below the heating curve, indicating a small degree of oxidation during heating. Both the Curie point at 580–600°C and the reversibility of the curves indicate that the preponderant low-coercivity magnetic mineral is magnetite.

[12] As magnetite is the largely dominant magnetic mineral in the sediment, we have used anhysteretic susceptibility (κ_{ARM}, see Appendix A) versus volume susceptibility (κ) and ARM versus IRM ratios to estimate the magnetic grain size [*King et al.*, 1982]. These ratios, plotted versus time as in Figure 4, largely covary indicating a negligible paramagnetic contribution to κ. They both indicate that the

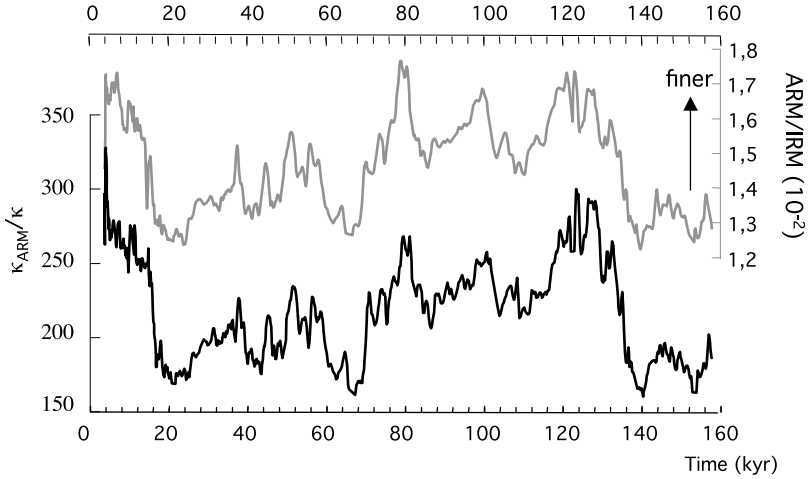

Figure 4. Magnetic grain size in core MD06-3067 expressed by the ratios ARM/IRM (in gray) and κ_{ARM}/κ (in black). Both show the same variations versus time.

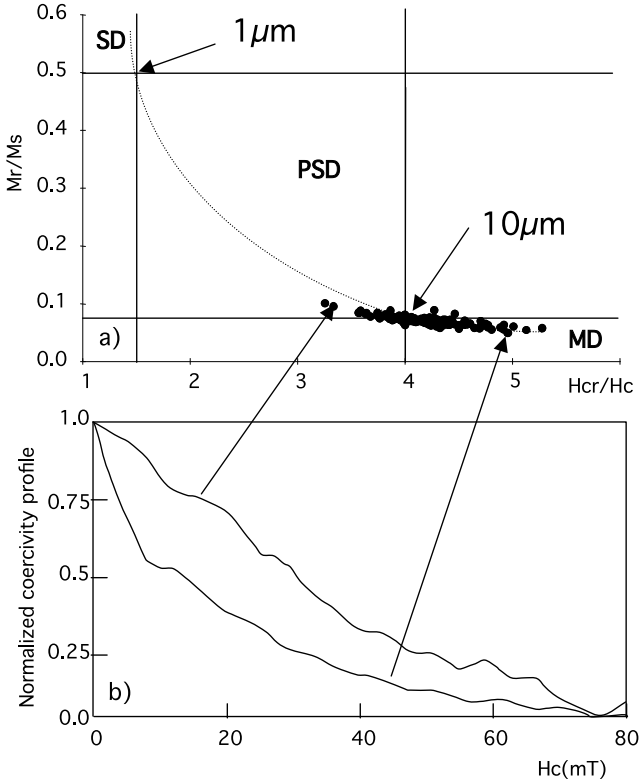

Figure 5. (a) Magnetic hysteresis parameters in core MD06-3067 reported as Mr/Ms versus Hcr/Hc ratios [*Day et al.*, 1977] with the hyperbole (solid line) corresponding to magnetite grain size distribution between SD (single domains), PSD (pseudosingle domains), and MD (multidomains). (b) Two coercivity profiles from FORC diagrams (profiles along Hu = 0) showing the different distribution of coercivities in samples characterized by the mean finest grains (top curve) and coarsest grains (bottom curve).

bottom of the core is characterized by the coarsest magnetic grains and a sharp decrease of the magnetic grain size is observed around 130–140 kyr (at termination II). There is then a progressive coarsening trend up to marine isotopic stage 2 (MIS2) with superimposed significant fluctuations. Termination I is also characterized by a sharp decrease in the grain size, which remains then relatively constant at the top of the sequence. When the hysteresis parameters are reported as magnetization ratio (Mrs/Ms) versus coercitive forces ratio (Hcr/Hc) [*Day et al.*, 1977], they confirm the variability of the grain size of magnetite. They also show that, in a general way, the mean sizes of these grains are relatively large, ranging between pseudosingle domain and multidomain areas (Figure 5a). For magnetites, this corresponds to average grain sizes of about 10 μm. FORC diagrams obtained from different horizons look very similar. However, the coercivity profiles (horizontal profile across the Hu = 0 line) of coarser intervals are clearly shifted toward lower ceorcivities than the finer intervals (Figure 5b). The latter are therefore constituted of a large spectrum of magnetic grain sizes with a large majority of multidomain grains.

[13] Among the three bulk magnetic parameters (Figure 6), IRM and κ largely covary. Relative changes in the amplitude ARM are slightly different, again illustrating changes in magnetic grain sizes as discussed above. These magnetic parameters vary rather regularly within a stable envelope. The $CaCO_3$ content in this core is relatively low, ranging between 14% and 24%. Although $CaCO_3$ is anticorrelated with the magnetic content, when susceptibility is corrected for this possible dilution effect [*Pouthiers and Gonthier*, 1978], the record still clearly documents the same variations as those observed in the uncorrected record (Figure 6). Except for a small difference around 30 kyr, the down-core patterns of Fe and Ti intensities normalized by Ca intensity and expressed as log ratios [*Weltje and Tjallingii*, 2008] are also very similar to the magnetic concentration (Figure 6). Therefore, the magnetic grains, Fe and Ti all trace the same terrigenous assemblage, the concentration of which varies in time independently from any carbonate dilution effect.

4.2. Anisotropy of the Low-Field Magnetic Susceptibility

[14] The crystalline anisotropy of magnetite, the main magnetic mineral in core MD06-3067, is very weak and shape anisotropy is dominant with the maximum susceptibility aligned with the long axis of the grain. In core MD06-3067, the analysis of the 'magnetic fabric' thus provides information about the preferential alignment of the elongated magnetite grains in the sediment.

[15] Only the uppermost 1.5 m of core MD06-3067 exhibits an elongated magnetic fabric aligned with the core

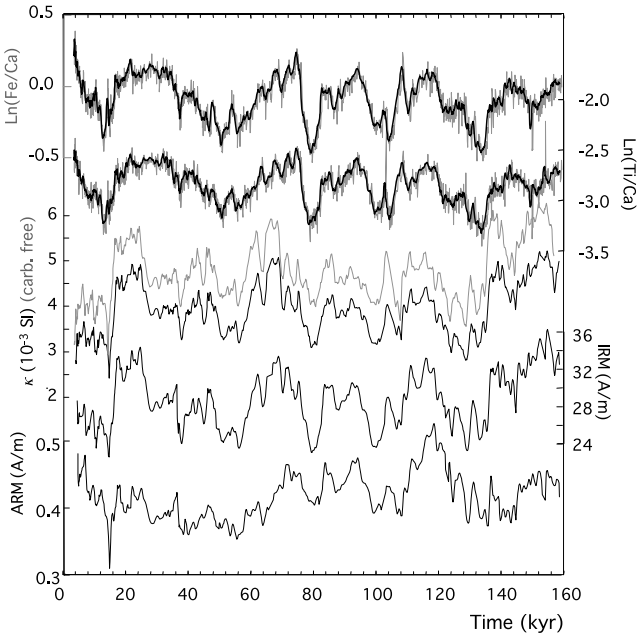

Figure 6. Ti/Ca and Fe/Ca log ratio (and a 7-points running average) and bulk magnetic parameter (κ, IRM and ARM) curves versus time in core MD06-3067. The magnetic susceptibility calculated on a carbonate-free basis is also reported on the same vertical scale as κ by the gray curve.

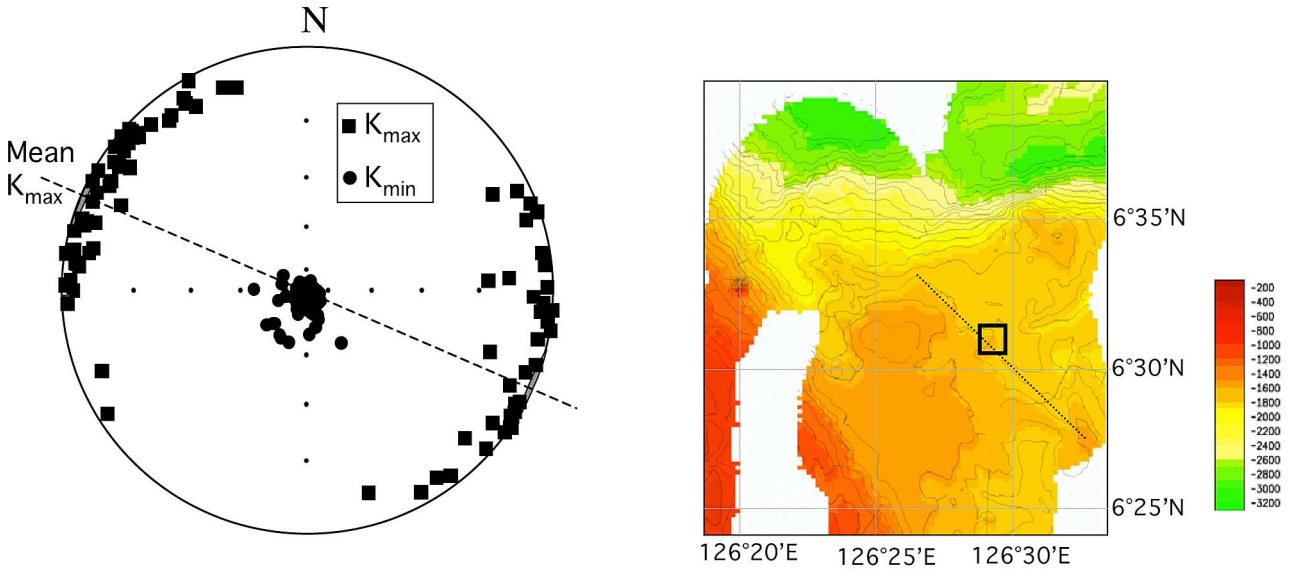

Figure 7. (left) Distribution of the principal axes of anisotropy (in geographic coordinates, see text): Kmin (black circles) and Kmax (black squares). The dashed line and the gray area illustrate the mean direction and associated ellipse of confidence for Kmax. (right) Bathymetric map obtained around the site (square) during the survey on board the R.V. *Marion Dufresne* using the multibeam echo sounder Thomson Seafalcon 11 and processed with Caraibes software [*Laj et al.*, 2006].

axis. This illustrates perturbation due to the piston during the coring process. The rest of the core is entirely characterized by an oblate anisotropy ellipsoid with minimum axes K_{min} close to the vertical, i.e., perpendicular to the bedding plane (I_{mean} = 85°) (Figure 7). This is typical for a sedimentary magnetic fabric acquired during deposition and possible subsequent compaction. Within the bedding plane, we observe that the maximum axes of the AMS ellipsoid (K_{max}) are rather well grouped, marking a magnetic lineation.

[16] In order to determine the real orientation of the magnetic lineation in geographical coordinates, i.e., the orientation of the core in the horizontal plane, we used the average direction of the stable component of the NRM (Characteristic Remanent magnetization (ChRM)), which is precisely determined after stepwise demagnetization with a mean angular deviation (MAD) angle never exceeding 5°. After reorientation of core MD06-3067, aligning the mean declination at 0°, the anisotropy lineation varies between 58° and 178° (80% of the data are between 80° and 133°) with an average direction around 113°. The directions of the principal axes K_{max} in geographical coordinates are reported in Figure 7.

4.3. Grain Size Measurements

[17] As an independent tool for deciphering changes in the bottom current flow speed, the sortable silt mean size was examined (see Appendix A). In core MD06-3067, the downcore record of sortable silt mean size shown in Figure 8 exhibits variations from about 22 μm to 29μm. As for the magnetic grain size, the coarsest grains are observed at the top of the core close to 20 kyr and the finest grains at the bottom of the core close to 120–130 kyr. The interpretation of the sortable silt mean diameter as a proxy of bottom current flow is corroborated by the disaggregated grain size distributions exemplified in Figure 8. In general, the shape of these distributions is determined by source material, boundary shear stress and the extent of flocculation [*McCave et al.*, 1995; *Curran et al.*, 2004]. The maximum grain size increases with boundary shear stress, suggesting that near-bed energy was higher in the glacial sample (II-130) compared to the interglacial sample (I-60), in line with the coarser sortable silt size and inferred stronger bottom current during this time interval. The slope of the fine portion (source slope) of the glacial and interglacial grain size distributions is similar (Figure 8) implying that the material originates from a single source throughout the time interval explored here.

5. Discussion and Conclusion

5.1. Orbitally Controlled Sedimentary Discharge

[18] As basaltic rocks are very rich in magnetites, the latter are abundant in oceanic sediments in the vicinity of basaltic sequences [*Kissel et al.*, 1999, 2009; *Mazaud et al.*, 2002]. Both titanium and iron are also present in large amounts in many different minerals constituting basaltic rocks. Consequently, a terrigenous fraction rich in magnetites, Ti and Fe often characterizes oceanic sediments partly fed by nearby basaltic sources [*Lavrov et al.*, 1973; *Kissel et al.*, 2009]. In core MD06-3067, magnetite concentration, Ti and Fe contents closely covary, thus indicating that they originate from nearby basaltic rocks. Both the magnetic grain size and the mean sortable silt size are significantly coarser than in open ocean environments distant from sediment source regions [e.g., *Bianchi and McCave*, 1999; *Hall et al.*, 2001, 2004; *Kissel et al.*, 2009]. This indicates

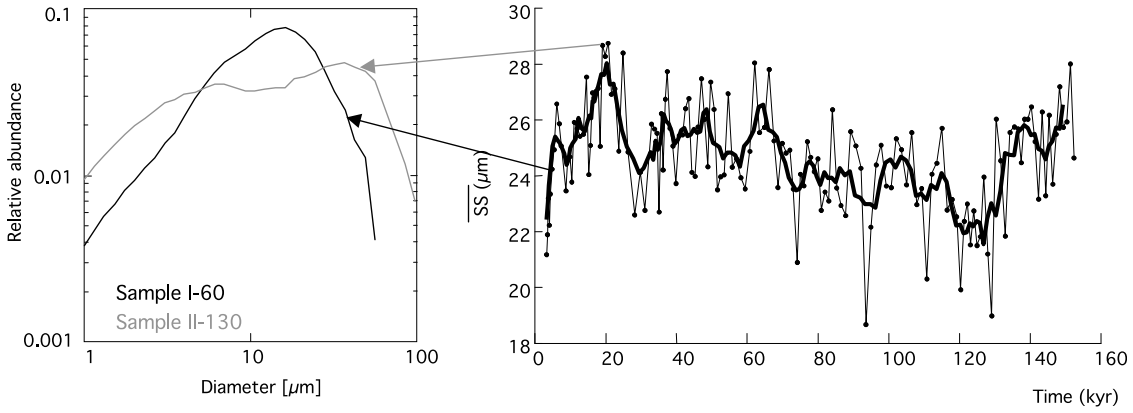

Figure 8. Inorganic mean grain size in core MD06-3067. (right) Sortable silt mean size (thin black curve) and running average curve (thick line) versus time. (left) Examples of two spectra obtained for fine (black curve) and coarse (gray curve).

that this basaltic source is very proximal to the coring site. Given the geology of the islands in this region and the location of the core, we infer that the detrital fraction originates from the basaltic rocks forming the large majority of the volcanic island of Mindanao [*Sajona et al.*, 1997]. The strong (33 Sv) southward directed surface (upper) Mindanao current causes the particles eroded from Mindanao to be largely transported southward. A canyon located north of our site could possibly receive part of the runoff sediments from Mindanao, but does not appear to be an impassable obstacle for the sediments to reach the coring site. In addition, the shelf in this area is very narrow, due to the presence of the very deep Philippine trench bordering the islands, thus making a significant contribution from resuspension of sediment from the shelf during sea level low stands very unlikely.

[19] Down-core variations in the abundance of magnetites are thus interpreted to directly reflect delivery of sediments from Mindanao Island, which, in turn, is used as a proxy for precipitation in the hinterland. The direct comparison of the total summer (1 June to 31 August) insolation curve at 30°N with the magnetite concentration curves indicates a clear relationship (Figure 9a). To better scrutinize this relationship, we performed a Blackman-Tukey spectral analysis using the Analyseries 2.0.3 software [*Paillard et al.*, 1996] on the records of κ and IRM. The spectra shown in Figure 9b indicate a broad and very significant maximum covering the obliquity and precession bands at 40 (obliquity) and 23 kyr (precession), respectively. These two cycles together control the fluctuations of the magnetic content off Mindanao i.e., changes in the East Asian summer monsoon intensity in this region. The other minor peaks in the curves at shorter periodicities are most likely not significant. The coherence and the phasing of the orbital parameters with the proxy records, were inferred from cross correlation between the different series. The precession and obliquity curves were obtained by filtering the insolation at 30°N shown in Figure 9a using 23 kyr and 40 kyr filters, respectively, and they were cross correlated with κ on one side and IRM on the other side.

[20] In all cases, a significant coherence (>95% confidence limit) is observed for each periodicity between the orbital curves and each proxy, thus confirming the influence of both precession and obliquity. A significant coherence peak is associated with a phase shift of about 160° and 170° in the precession and the obliquity bands, respectively. This implies that the runoff from Mindanao is almost anticorrelated with northern hemisphere insolation, i.e., maximum precipitation on this island roughly coincides with precession and obliquity minima as calculated at 30°N. The small time shift of about 1–2 kyr between the two is short compared to the uncertainties of the age model and may not be significant. Therefore no firm conclusion can be drawn about it at the moment. This clear anticorrelation may appear inconsistent with the common association of strong boreal summer insolation with increased monsoon precipitation. However, *Braconnot et al.* [2008], have inferred from GCM runs that precipitation in the area of Mindanao was lower during the insolation maximum at 126 kyr BP and stronger during the insolation minimum at 115 ka, while the situation was reverse on the Asian continent (Figure 10). Models therefore suggest that in southeast Asia and in the western equatorial Pacific, there is a contrast between precipitation rates on land and in the marine realm.

[21] In summary, the results from core MD06-3067 support the suggestion of a control of the Asian summer monsoon by insolation in the western equatorial Pacific. In addition, this record from the open ocean offers a first experimental observation of lower precipitation regime on the ocean side than on the continent during boreal insolation maxima, corroborating GCM model results [*Braconnot et al.*, 2008]. This would illustrate a change of the rain belt position during summer. Other proxies from the same site show that during the same periods, the winter wind stress was also intensified, giving rise to enhanced upwelling off Mindanao (T. Bolliet et al., submitted manuscript, 2010). The seasonality contrast with longer winter seasons and a relative southward shift of the ITCZ during summer months can account for both effects. As emphasized by *Wang* [2009], each record is influenced by both global and regional components, the latter originating from regional sea-land thermal contrasts. Obviously more records are

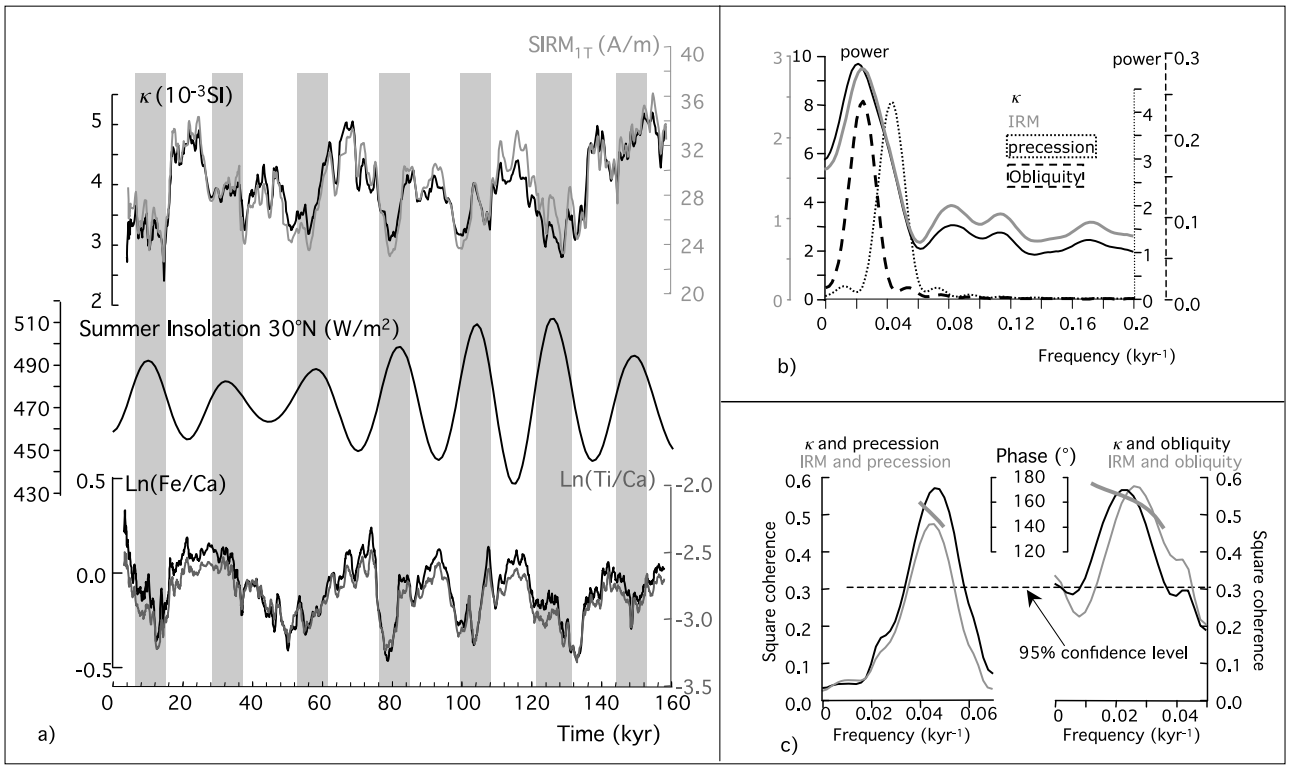

Figure 9. Relationship between magnetic concentration in core MD06-3067 and insolation. (a) Comparison between IRM, κ, Ln(Fe/Ca), Ln(Ti/Ca) (both reported as 7-points running average curves), and the summer (1 June to 31 August) mean insolation curve calculated at 30°N using *Laskar et al.* [2004] solution; (b) Blackman-Tukey spectrum analysis calculated using Analyseries software [*Paillard et al.*, 1996] for κ (black), IRM (gray), and the insolation shown in Figure 9a after filtering at 23 kyr (named "precession," dotted line) and 40 kyr (named "obliquity," dashed line); (c) squared coherence between κ (black), IRM (gray), and the 23 kyr-filtered insolation curve on the left and between κ, IRM, 40 kyr-filtered periodicity on the right. The phases between the magnetic parameters and the insolation ones are reported in degrees for the time domain in which the curves are significantly correlated.

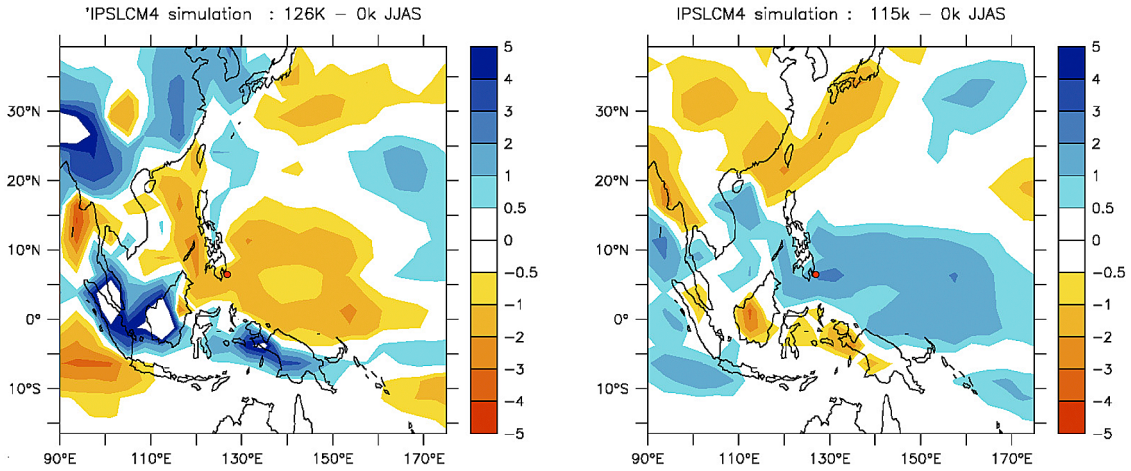

Figure 10. Differences with 0 ka precipitation over the area (mm/d) for two characteristic periods: (left) 126 ka (maximum northern summer insolation) and (right) 115 ka (minimum northern summer insolation). These simulations were made using the IPSL_CM4 ocean-atmosphere coupled models [*Braconnot et al.*, 2008].

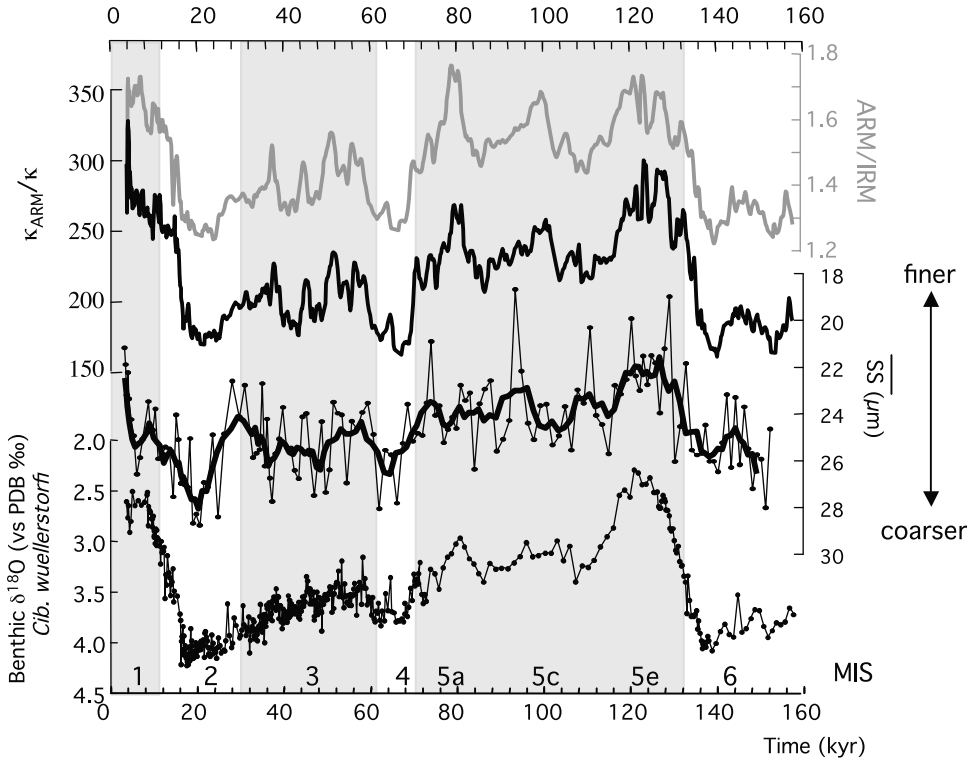

Figure 11. Comparison of temporal variations in the mean size of sortable silt and magnetic fraction with the benthic δ^{18}O curve in core MD06-3067. The vertical scale for sortable silt has been inverted to report the finer grains upward and the coarser ones downward.

needed to improve our understanding of the system and to better constrain models.

5.2. Near Bottom Current Strength

[22] Sediment particles larger than 10 μm, on average, behave noncohesively and are size sorted by hydrodynamic processes [*McCave et al.*, 1995]. The mean size of this "sortable silt" fraction thus reflects the degree to which deep sea sediments have been reworked by currents and is widely used as a proxy of bottom current strength [*McCave and Hall*, 2006, and references therein]. In core MD06-3067, the down-core record of sortable silt mean size parallels tightly the magnetic grain size record described above, and both show a clear glacial-interglacial variability with coarser grains (stronger mean flow speeds) during glacial periods and finer grains (weaker flow) during interglacials. The close match between SS, magnetic grain sizes and benthic δ^{18}O holds beyond these mere glacial-interglacial contrasts, implying a close coupling between deep water flow at this site and global climate.

[23] The presence of bottom current acting during the deposition of the particles can also be assessed by the study of the anisotropy of magnetic susceptibility [*Rees*, 1961, 1965; *Hamilton and Rees*, 1970; *Ellwood and Ledbetter*, 1977; *Kissel et al.*, 1997]. Because bottom currents, when they exist, statistically align the elongated magnetic particles during deposition, preferential alignment of the long axes of the anisotropy ellipsoids indicates the orientation of the bottom currents. In core MD06-3067, as we described above, the magnetic lineation observed in the deposition plane is oriented around 113° with a dispersion consistent with the local topography (about 130–135°) as surveyed with the multibeam of the R. V. *Marion Dufresne* during the Marco Polo 2 cruise (Figure 7) [*Laj et al.*, 2006]. Since bottom flow is strongly dependent on the seafloor topography, this alignment between topography and magnetic particles confirms that deposition occurred under the influence of bottom currents. The statistical alignment of the particles throughout the entire length of the core suggests that a bottom current was continuously present during the last 160 kyrs. This, in turn, also implies that changes in the mean grain size are a more faithful recorder of variations in bottom current intensity than changes in the anisotropy parameters.

[24] None of these methods yields a *quantitative* record of bottom current strength. However, as observed in Figure 11, the magnetic and grain size proxies of bottom current flow both clearly indicate relative changes in the strength of the bottom currents with invigorated glacial bottom currents at 1574 m off the SE Philippines, compared to weaker interglacial flow. Because the actual direction of flow cannot be determined using these methods, we follow here two lines of evidence to argue that most, if not all, bottom current variability observed in core MD06-3067 is due to changes in the northward flow of circum Antarctica-sourced waters. First, studies of the present-day oceanography suggest that the deeper part of the NGCUC flows across the equator (where it becomes the MUC) transporting AAIW [*Tsuchiya*,

1991; *Fine et al.*, 1994; *Qu and Lindstrom*, 2004], and possibly the upper layer of Pacific Deep Water [*Saikku et al.*, 2009] into the North Pacific along the Mindanao coast. This is also consistent with the interpretation of regional subsurface hydrography proposed by *Stott et al.* [2007]. Second, based on sortable silt flow speed and benthic $\delta^{13}C$ water mass property records in a core sampling the deep western boundary current (3290 m water depth east of New Zealand), *Hall et al.* [2001] reconstructed greater Pacific ventilation during Pleistocene glacial periods.

[25] We note, however, that *McCave et al.* [2008] inferred near-constant glacial-interglacial water mass structure and vigor of inflow from depth profiles (1200 to 4800 m water depth) of benthic $\delta^{13}C$ and sortable silt size on North Chatham Rise.

[26] While the precise origin of bottom currents off Mindanao is somewhat ill-constrained (see above), the close match between benthic $\delta^{18}O$ and records of bottom flow speed yields evidence for a close coupling between global climate and deep circulation in the western equatorial Pacific on at least orbital timescales. The records and interpretation presented here are consistent with some, but not all reconstructions of Deep Western Boundary Current ventilation and flow speed. Efforts are underway to better constrain the chemical properties, and thus the origin of the near bottom water masses off Mindanao.

[27] In summary, two main conclusions are drawn from this investigation of the long-term changes in the sedimentary parameters of core MD06-3067. First, significant changes in the runoff from Mindanao island as documented by variations in the concentration of the magnetic fraction are clearly linked to a combined effect of precession and obliquity. This implies that the summer monsoon intensity in this region is controlled by both orbital cycles. The antiphase between orbital and proxy records constitutes the first experimental evidence that this area is subject to a shift of the rain belt with lower precipitation rates during northern summer insolation maxima. This is consistent with the results obtained from GCM simulations. Second, records of sortable silt mean size and magnetic grain sizes provide valuable information about the strength of bottom currents on an orbital scale. Both proxies indicate stronger glacial deepwater flow compared to interglacial times, typical of a southern source type signal.

Appendix A

[28] The low field susceptibility was systematically measured on all the cores on board the R. V. *Marion Dufresne* during the MD155-Marco Polo2 cruise. The measurements were made with a Bartington point sensor, sensitive to the very first millimeter at the surface of the sediment. In order to get more representative data, although at lower resolution, we measured again the low-field magnetic susceptibility in the laboratory at LSCE on u channels with a 45 mm diameter MS2-C Bartington coil. The data were generated every 2 cm with a resolution close to 4 cm and they were normalized by the volume to get the volume susceptibility (κ).

[29] The natural remanent magnetization (NRM) was measured using a 755-R 2G cryogenic pass through magnetometer, equipped with a high-resolution set of coils and placed in the μ-metal shielded room of LSCE. An in-line alternating field (AF) demagnetization unit was used for the stepwise demagnetization at 5, 10, 15, 20, 25, 30, 35, 40, 50, 60 and 80 mT. After demagnetization at 80 mT, about 97% of the initial magnetization was removed. Measurements were made every 2 cm with a resolution of about 4 cm. The direction of the Characteristic Remanent Magnetization (ChRM) was determined using principal component analysis through the results obtained from the demagnetization process [*Kirschvink*, 1980; *Mazaud*, 2005]. For this calculation, we used 10 steps of demagnetization except at very few horizons where we used 9 steps. MAD angles very rarely exceed 5° (with a maximum at 8°) showing that the direction of magnetization is very stable upon demagnetization.

[30] The Anhysteretic Remanent (ARM) and Isothermal Remanent (IRM) magnetizations were acquired and demagnetized also on u channels using the same method and instruments. ARM was acquired along the vertical geographic axis in a peak alternating field of 100 mT and a steady bias field of 50 μT. During acquisition, the sampled were translated through the coils at a speed of about 1 cm/s, following *Brachfeld et al.* [2004]. After acquisition, the ARM was then progressively demagnetized using 10 steps at 10, 15, 20, 25, 30, 35, 40, 50, 60, and 80 mT. Saturated IRM (SIRM) was then acquired, also along the vertical geographical axis in six steps (0.05, 0.1, 0.2, 0.3, 0.5 and 1 T) using a 2G 1.6 m long pulsed solenoid. Backfield to 0.3 T was applied after saturation in order to calculate the S-ratio ($S_{-0.3T} = abs(IRM_{-0.3T}/IRM_{1T})$). SIRM was stepwise demagnetized using 10 steps (5, 10, 20, 25, 30, 35, 40, 50, 60, 80 mT). During the demagnetization of NRM, ARM and IRM, the u channels were translated at a speed of about 4 cm/s through the demagnetization coils. All the data were acquired using softwares developed at LSCE, which allow to considerably reduce the translation speed during the measurements, while the u channel passes through the pickup coil. This is particularly adapted to the measurements of very high magnetizations because the reduced translation speed allows to reliably count the flux jumps.

[31] From the ARM and IRM stepwise demagnetizations, we could calculate the median destructive fields of these two remanent magnetizations. They are labeled Hmd_{ARM} and Hmd_{IRM}. Together with the S-ratio, they both give information about the coercivity spectrum of the magnetic particles included in the sediment.

[32] ARM, κ and IRM were used to estimate changes in the average magnetic grain size. To calculate the ratio ARM/κ ratio, the ARM data are presented as an anhysteretic susceptibility (κ_{ARM}) by normalizing ARM by the DC biasing field.

[33] Small chips were also taken at the surface of the sediment, at 10 cm intervals. After drying, they were used for the measurements of the hysteresis parameters using an AGM 2900 from Princeton Measurements Corporation. The hysteresis loops were made between +1 and −1 T. After adjustment of the high field slope, giving access to the high-field magnetic susceptibility, the saturation magnetization (Ms), the remanent saturation magnetization (Mrs), the

coercitive field (Hc) were calculated. Ms and Mrs were normalized by the mass of the sample. The remanent coercitive field (Hcr) was then determined by a remanent curve starting by a saturation at 1T followed by a stepwise decreasing field, opposed to the saturating one.

[34] AMS is described by a symmetric tensor of second rank which in turn may be visualized as an ellipsoid with principal axes K_{max}, K_{int}, K_{min} ($K_{max} > K_{int} > K_{min}$). Depending on the magnetic minerals, AMS reflect the orientation of elongated particles or crystal lattices. Magnetites have a weak crystalline anisotropy and their shape anisotropy is dominant with the maximum susceptibility aligned with the long axis of the grain. The analysis of the magnetic fabric thus provides information about the preferential alignment of the elongated magnetite grains in the sediment. AMS measurements were made in core MD06-3067 using cubic samples with a KLY-3 Agico anisotropy spinner magnetometer. We have carefully checked that there is no relation between the lineation and the direction along which the samples were pushed into the sediment, so the observed lineation is not related to our sampling technique. The mean orientation of the principal axes of anisotropy was calculated using the method reported by *Jelinek* [1978].

[35] All these parameters give access to the magnetic content of the sediments in terms of nature of the magnetic minerals, their grain size and their concentration (see text).

[36] Disaggregated inorganic grain size distributions (DIGS) were determined on the organic matter and carbonate-free (quantitatively removed by H_2O_2 and HCl, respectively) terrigenous sediment fraction using a Coulter Multisizer IIe electroresistance particle size analyzer. This Coulter Counter at Dalhousie University is equipped with 30, 140 and 400 um aperture tubes. Details of the analytical method are given by *Curran et al.* [2004]. As per *McCave et al.* [1995], the sortable silt mean size (SS) presented here is defined as the mean of the 10–63 μm grain size range.

[37] **Acknowledgments.** We are very grateful to the crew of the R.V. *Marion Dufresne*, who helped us a lot during the cruise under the command of Captain J. P. Hedrich. We also thank all the team from the French Polar Institute (IPEV). This cruise is part of the IMAGES program. We are grateful to Camille Wandres (LSCE), who helped with the measurements of the magnetic properties, and to Aurélie Van Toer (LSCE) for her participation to the sortable silt measurements. A. Hill and A. Roy (Dalhousie University) helped with the grain size analyses. U. Röhl and colleagues at Marum (Bremen University) gave valuable advice for using their Avaatech XRF scanner. Ph. Robion (Université de Cergy) helped with the statistical treatment of the magnetic anisotropy data. We are grateful to L. Vigliotti and an anonymous reviewer for their advices to improve the manuscript. Funds for laboratory analyses in France were provided by the French Atomic Energy Commission and the Centre National de la Recherche Scientifique. Analytical work at Dalhousie was funded by NSERC Canada and the Canadian Institute for Advanced Research (CIFAR). In Germany, analyses were funded by the German Research Foundation (DFG) through the grant Ku649/26-1. This is LSCE contribution 4201.

References

Bianchi, G. G., and I. N. McCave (1999), Holocene periodicity in North Atlantic climate and deep-ocean flow south of Iceland, *Nature*, *397*, 515–517, doi:10.1038/17362.

Brachfeld, S., C. Kissel, C. Laj, and A. Mazaud (2004), Viscous behavior of U channels during acquisition and demagnetization of remanences: Implications for paleomagnetic and rock-magnetic investigations, *Phys. Earth Planet. Inter.*, *145*, 1–8, doi:10.1016/j.pepi.2003.12.011.

Braconnot, P., C. Marzin, L. Gregoire, E. Mosquet, and O. Marti (2008), Monsoon response to changes in Earth's orbital parameters: Comparisons between simulations of the Eemian and of the Holocene, *Clim. Past Discuss.*, *4*, 459–493, doi:10.5194/cpd-4-459-2008.

Broecker, W. S., W. C. Patzert, J. R. Toggweiler, and M. Stuiver (1986), Hydrography, chemistry and radioisotopes in the Southeast Asian Basins, *J. Geophys. Res.*, *91*, 14,345–14,354, doi:10.1029/JC091iC12p14345.

Curran, K. J., P. S. Hill, T. M. Schell, T. G. Milligan, and D. J. W. Piper (2004), Inferring the mass fraction of floc-deposited mud: Application to fine-grained turbidites, *Sedimentology*, *51*, 927–944, doi:10.1111/j.1365-3091.2004.00647.x.

Day, R., M. Fuller, and V. A. Schmidt (1977), Hysteresis properties of titano-magnetite: Grain-size and compositional dependence, *Phys. Earth Planet. Inter.*, *13*, 260–267, doi:10.1016/0031-9201(77)90108-X.

Ellwood, B. B., and M. T. Ledbetter (1977), Antarctic bottom water fluctuations in the Vema Channel: Effects of velocity changes on particle alignment and size, *Earth Planet. Sci. Lett.*, *35*, 189–198, doi:10.1016/0012-821X(77)90121-2.

Fine, R. A., R. Lukas, F. M. Bingham, M. J. Warner, and R. H. Gammon (1994), The western equatorial Pacific: A water mass crossroads, *J. Geophys. Res.*, *99*(12), 25,063–25,080, doi:10.1029/94JC02277.

Hall, I. R., I. N. McCave, N. J. Shackleton, G. P. Weedon, and S. E. Harri (2001), Intensified deep Pacific inflow and ventilation in Pleistocene glacial times, *Nature*, *412*, 809–812, doi:10.1038/35090552.

Hall, I. R., G. G. Bianchi, and J. R. Evans (2004), Centennial to millennial scale Holocene climate-deep water linkage in the North Atlantic, *Quat. Sci. Rev.*, *23*, 1529–1536, doi:10.1016/j.quascirev.2004.04.004.

Hamilton, N. D., and A. I. Rees (1970), The use of magnetic fabric in paleocurrent estimation, in *Paleogeophysics*, edited by S. K. Runcorn, pp. 445–464, Academic, Orlando, Fla.

Jelinek, V. (1978), Statistical processing of anisotropy of magnetic susceptibility measured on groups of specimens, *Stud. Geophys. Geod.*, *22*, 50–62, doi:10.1007/BF01613632.

Kashino, Y., M. Aoyama, T. Kawano, N. Hendiarti, Syaefudin, Y. Anantasena, K. Muneyama, and H. Watanabe (1996), The water masses between Mindanao and New Guinea, *J. Geophys. Res.*, *101*, 12,391–12,400, doi:10.1029/95JC03797.

King, J. W., S. K. Banerjee, J. Marvin, and Ö. Özdemir (1982), A comparison of different magnetic methods for determining the relative grain size of magnetite in natural materials: Some results from lake sediments, *Earth Planet. Sci. Lett.*, *59*, 404–419, doi:10.1016/0012-821X(82)90142-X.

Kirschvink, J. L. (1980), The least-squares line and plane and the analysis of paleomagnetic data, *Geophys. J. R. Astron. Soc.*, *62*, 699–718.

Kissel, C., C. Laj, B. Lehman, L. Labeyrie, and V. Bout-Roumazeilles (1997), Changes in the strength of the Iceland–Scotland Overflow Water in the last 200,000 years: Evidence from magnetic anisotropy analysis of core SU90–33, *Earth Planet. Sci. Lett.*, *152*, 25–36, doi:10.1016/S0012-821X(97)00146-5.

Kissel, C., C. Laj, L. Labeyrie, T. Dokken, A. Voelker, and D. Blamart (1999), Rapid climatic variations during marine isotopic stage 3: Magnetic analysis of North Atlantic sediments, *Earth Planet. Sci. Lett.*, *171*, 489–502.

Kissel, C., C. Laj, T. Mulder, C. Wandres, and M. Cremer (2009), The magnetic fraction: A tracer of deep water circulation in the North Atlantic, *Earth Planet. Sci. Lett.*, *288*, 444–454, doi:10.1016/j.epsl.2009.10.005.

Laj, C., et al. (2006), IMAGES XIV, MD155-Marco Polo 2 cruise report OCE/2006/06, in *Les rapports de campagne à la mer*, 55 pp., Inst. Polaire Fr., Plouzané, France.

Laskar, J., P. Robutel, F. Joutel, M. Gastineau, A. C. M. Correia, and B. Levrard (2004), A long-term numerical solution for the insolation quantities of the Earth, *Astron. Astrophys.*, *428*, 261–285, doi:10.1051/0004-6361:20041335.

Lavrov, V. M., V. K. Nikolayeva, and M. S. Barash (1973), Titanium in the quaternary deposits of the Atlantic Ocean, *Oceanology*, Engl. Transl., *13*, 57–62.

Lindstrom, E., R. Lukas, R. Fine, E. Firing, S. Godfrey, G. Meyers, and M. Tsuchiya (1987), The western equatorial Pacific Ocean circulation study, *Nature*, *330*, 533–537, doi:10.1038/330533a0.

Lukas, R., E. Firing, P. Hacker, P. L. Richardson, C. A. Collins, R. Fine, and R. Gammon (1991), Observations of the Mindanao current during the western equatorial, Pacific Ocean

circulation study, *J. Geophys. Res.*, *96*(C4), 7089–7104, doi:10.1029/91JC00062.

Mazaud, A. (2005), User-friendly software for vector analysis of the magnetization of long sediment cores, *Geochem. Geophys. Geosyst.*, *6*, Q12006, doi:10.1029/2005GC001036.

Mazaud, A., M. A. Sicre, U. Ezat, J. J. Pichon, J. Duprat, C. Laj, C. Kissel, L. Beaufort, E. Michel, and J. L. Turon (2002), Geomagnetic assisted stratigraphy and SST changes in core MD94-103 (southern Indian Ocean): Possible implications for North-South climatic relationships around H4, *Earth Planet. Sci. Lett.*, *201*, 159–170.

McCave, I. N., and I. R. Hall (2006), Size sorting in marine muds: Processes, pitfalls, and prospects for paleoflow-speed proxies, *Geochem. Geophys. Geosyst.*, *7*, Q10N05, doi:10.1029/2006GC001284.

McCave, I. N., B. Manighetti, and S. G. Robinson (1995), Sortable silt and fine sediment size/composition slicing: Parameters for paleocurrent speed and paleoceanography, *Paleoceanography*, *10*, 593–610, doi:10.1029/94PA03039.

McCave, I. N., L. Carter, and I. R. Hall (2008), Glacial-interglacial changes in water mass structure and flow in the SW Pacific Ocean, *Quat. Sci. Rev.*, *27*(19–20), 1886–1908, doi:10.1016/j.quascirev.2008.07.010.

Paillard, D., L. Labeyrie, and P. Yiou (1996), Macintosh program performs time-series analysis, *Eos Trans. AGU*, *77*, 379, doi:10.1029/96EO00259.

Pouthiers, J., and E. Gonthier (1978), Sur la susceptibilité magnétique des sédiments, indicateurs de la dispersion du matériel volcanoclastique à partir de l'Islande et des Faeroes, *Bull. Inst. Géol. Bassin Aquitaine*, *23*, 214–226.

Qu, T. D., and E. J. Lindstrom (2004), Northward intrusion of Antarctic intermediate water in the western Pacific, *J. Phys. Oceanogr.*, *34*(9), 2104–2118, doi:10.1175/1520-0485(2004)034<2104:NIOAIW>2.0.CO;2.

Rees, A. I. (1961), The effects of water currents on the magnetic remanence and anisotropy of susceptibility of some sediments, *Geophys. J. R. Astron. Soc.*, *6*, 235–251.

Rees, A. I. (1965), The use of anisotropy of magnetic susceptibility in the estimation of sedimentary fabric, *Sedimentology*, *4*, 257–271, doi:10.1111/j.1365-3091.1965.tb01550.x.

Richter, T. O., S. Van der Gaast, B. Koster, A. Vaars, R. Gieles, H. De Stigter, H. De Haas, and T. C. E. vanWeering (2006), The Avaatech XRF core scanner: Technical description and applications to NE Atlantic sediments, in *New Techniques in Sediment Core Analysis. Special Publication*, vol. 267, edited by R. G. Rothwell, pp. 39–50, Geol. Soc., London.

Ruth, U., et al. (2007), "EDML1": A chronology for the EPICA deep ice core from Dronning Maud Land, Antarctica, over the last 150 000 years, *Clim. Past*, *3*, 475–484.

Saikku, R., L. Stott, and R. Thunell (2009), A bi-polar signal recorded in the western tropical Pacific: Northern and southern hemisphere climate records from the Pacific warm pool during the last Ice Age, *Quat. Sci. Rev.*, *28*, 2374–2385, doi:10.1016/j.quascirev.2009.05.007.

Sajona, F. G., H. Bellon, R. C. Maury, M. Pubellier, R. D. Quebral, J. Cotton, F. E. Bayon, E. Pagado, and P. Pamatian (1997), Tertiary and Quaternary magmatism in Mindanao and Leyte (Philippines): Geochronology, geochemistry and tectonic setting, *J. Asian Earth Sci.*, *15*(2–3), 121–153.

Stott, L., A. Timmermann, and R. Thunell (2007), Southern hemisphere and deep-sea warming led deglacial atmospheric CO_2 rise and tropical warming, *Science*, *318*, 435–438, doi:10.1126/science.1143791.

Talley, L. D. (2007), *Hydrographic Atlas of the World Ocean Circulation Experiment (WOCE)*, vol. 2, *Pacific Ocean*, edited by M. Sparrow et al., Int. WOCE Proj. Off., Southampton, U. K.

Toole, J. M., R. C. Millard, Z. Wang, and S. Pu (1990), Observations of the Pacific North Equatorial Current Bifurcation at the Philippines coast, *J. Phys. Oceanogr.*, *20*, 307–320, doi:10.1175/1520-0485(1990)020<0307:OOTPNE>2.0.CO;2.

Tsuchiya, M. (1991), Flow path of the Antarctic Intermediate Water in the western equatorial South Pacific Ocean, *Deep Sea Res., Part A*, *38*, S273–S279.

Wang, P. (2009), Global monsoon in a geological perspective, *Chin. Sci. Bull.*, *54*(7), 1113–1136, doi:10.1007/s11434-009-0169-4.

Wang, P. X., S. Clemens, L. Beaufort, P. Braconnot, G. Ganssen, Z. M. Jian, P. Kershaw, and M. Sarnthein (2005), Evolution and variability of the Asian monsoon system: State of the art and outstanding issues, *Quat. Sci. Rev.*, *24*, 595–629, doi:10.1016/j.quascirev.2004.10.002.

Weeks, R., C. Laj, L. Endignoux, M. Fuller, A. Roberts, R. Manganne, E. Blanchard, and W. Goree (1993), Improvements in long-core measurement techniques: Applications in palaeomagnetism and palaeoceanography, *Geophys. J. Int.*, *114*, 651–662, doi:10.1111/j.1365-246X.1993.tb06994.x.

Weltje, G. J., and R. Tjallingii (2008), Calibration of XRF core scanners for quantitative geochemical logging of sediment cores: Theory and application, *Earth Planet. Sci. Lett.*, *274*, 423–438, doi:10.1016/j.epsl.2008.07.054.

T. Bolliet, A. Holbourn, and W. Kuhnt, Institut für Geowissenschaften, Christian-Albrechts-Universität, D-24118 Kiel, Germany.

P. Braconnot, C. Kissel, and C. Laj, Laboratoire des Sciences du Climat et de l'Environnement/IPSL, CEA-CNRS-UVSQ, Avenue de la Terrasse, F-91198 Gif-sur-Yvette, CEDEX, France. (Catherine.Kissel@lsce.ipsl.fr)

P. Hill and M. Kienast, Department of Oceanography, Dalhousie University, Halifax, NS B3H 4R2, Canada.